INL/EXT-10-19683

Aerosol Resuspension Model for MELCOR for Fusion and Very High Temperature Reactor Applications

B. J. Merrill and P. W. Humrickhouse

January 2011

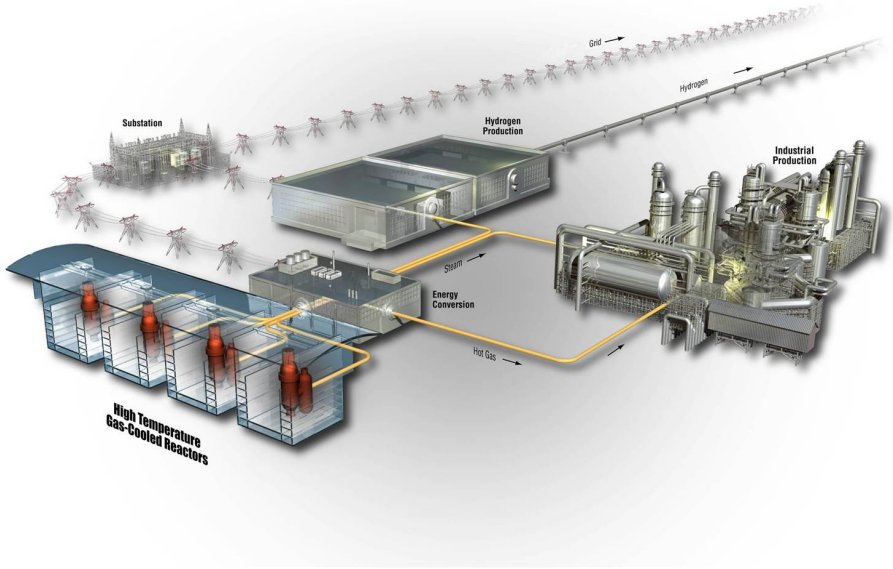

The INL is a
U.S. Department of Energy
National Laboratory
operated by
Battelle Energy Alliance

Idaho National Laboratory

INL/EXT-10-19683

Aerosol Resuspension Model for MELCOR for Fusion and Very High Temperature Reactor Applications

B. J. Merrill and P. W. Humrickhouse

January 2011

Idaho National Laboratory
Next Generation Nuclear Plant Project
Idaho Falls, Idaho 83415

Prepared for the
U.S. Department of Energy
Office of Nuclear Energy
Under DOE Idaho Operations Office
Contract DE-AC07-05ID14517

Next Generation Nuclear Plant Project

Aerosol Resuspension Model for MELCOR for Fusion and Very High Temperature Reactor Applications

INL/EXT-10-19683

January 2011

Approved by:

Brad J. Merrill Lead Author	1/3/2011 Date
Paul W. Humrickhouse Author/Technical Expert	1-3-2011 Date
Lee C. Cadwallader Peer Reviewer	01-03-2011 Date
Hans Gougar Responsible Manager	01-03-2011 Date

ABSTRACT

Dust is generated in fusion reactors from plasma erosion of plasma facing components within the reactor's vacuum vessel during reactor operation. This dust collects in cooler regions on interior surfaces of the vacuum vessel. Because this dust can be radioactive, toxic, and/or chemically reactive, it poses a safety concern, especially if mobilized by the process of resuspension during an accident and then transported as an aerosol thoughout the reactor confinement building, and possibly released to the environment. MELCOR is a computer code used at Idaho National Laboratory to model aerosol transport for safety consequence analysis. A primary reason for selecting MELCOR for this application is its aerosol transport capabilities. The Idaho National Laboratory Fusion Safety Program organization has made fusion-specific modifications to MELCOR. Recent modifications include the implementation of aerosol resuspension models in MELCOR 1.8.5 for Fusion. This paper presents the resuspension models adopted, and the initial benchmarking of these models.

CONTENTS

FIGURES

TABLES

Aerosol Resuspension Model for MELCOR for Fusion and Very High Temperature Reactor Applications

1. INTRODUCTION

Dust is generated in fusion reactors from plasma erosion of plasma facing components within the reactor's vacuum vessel during reactor operation. This dust collects in cooler regions on interior surfaces of the vacuum vessel. Dust is also be generated in very high temperature fission reactors such as in pebble bed reactors from core pebbles scrapping against reactor vessel walls or against each other during operation. This dust is transported and deposited throughout the reactor cooling system by the helium coolant. Because this dust can be radioactive, toxic, and or chemically reactive, it posses a safety concern. The dust can be mobilized by the process of resuspension during an accident, such as during a loss-of-coolant accident, and be transported as aerosols thoughout the reactor confinement building, and possibly released to the environment.

One computer code used at Idaho National Laboratory (INL) to model aerosol transport for safety consequence analysis is the MELCOR code. The MELCOR thermal-hydraulics code is currently under development at the Sandia National Laboratory for the U.S. Nuclear Regulatory Commission. The MELCOR code is used to model the progression of severe accidents in light water nuclear reactors. Modified version of this computer code have been developed at INL for both fusion (Merrill, Humrickhouse, and Moore 2009) and pebble bed reactor applications (Merrill 2008). Because aerosols are an important safety concern for both reactor concepts and because the MELCOR code does not presently contain any aerosol resuspension models, mechanistic models were sought that will give an estimate of quantity of aerosol mass deposited on a given surface during normal operation that will be resuspended in the coolant during accident conditions. Two models were adopted and implemented in MELCOR 1.8.5. These resuspension models are those proposed by Vainshtein (1997) and Reeks and Hall (2001). The report sections that follow describe the physics and equations upon which these models are based, the development and testing of the FORTRAN code for these models, and implementation and testing of these models in the MELCOR code.

2. VAINSHTEIN RESUSPENSION MODEL

As stated in Vainshtein (1997), the Vainshtein resuspension model, sometimes referred to in literature as the Vainshtein-Ziskind-Fichman-Gutfinger (VZFG) model, treats the re-entrainment of a particle from a surface by turbulent fluid drag forces. This model employs a potential well model developed by Reeks, Reed, and Hall (1988) and introduces a definition of the tangential pull-off force required to separate a particle from a surface. The determination of the tangential pull-off force is based on a nonlinear model of a particle undergoing stream-wise oscillations on a surface, produced by turbulent fluid drag forces, while being restrained by a linear spring like surface adhesive force. Vainshtein's derived resuspension rate constant—p (s^{-1})—is

$$p = f_o \exp\left(-\frac{F_{a\tau}^{4/3}}{F_d^{4/3}} \right) \tag{1}$$

where f_o is the frequency of particle oscillation (s^{-1}), $F_{a\tau}$ is the tangential pull-off force (N), and F_d is the fluid turbulent drag force (N).

The particle oscillation frequency adopted by Vainshtein is that derived experimentally by Reeks (1988):

$$f_o = \frac{\rho_f u_\tau^2}{300\,\mu_f} \tag{2}$$

where μ_f is fluid dynamic viscosity (kg/m-s), ρ_f is the fluid density (kg/m^3), and u_τ (m/s) is the fluid tangential friction velocity (m/s), which is equal to

$$u_\tau = \sqrt{C_f / 2}\; V_f \tag{3}$$

where, C_f is the fluid friction factor at the surface and V_f is the fluid bulk velocity (m/s).

The turbulent drag force defined by Vainshtein equals

$$F_d = C_d \rho u_\tau^2 R^2 \tag{4}$$

where C_d can be calculated from Vainshtein (1997) to be ~3.06, and R (m) is the particle radius (m).

Vainshtein (1997) derived the tangential pull-off force to be

$$F_{a\tau} = 9.3 \frac{\Delta\gamma^{4/3} R^{2/3}}{k^{1/3}} \tag{5}$$

where $\Delta\gamma$ is the surface (adhesive) energy, and k is the elastic constant. The surface energy is an experimentally derived quantity, while the elastic constant is given by

$$k = \frac{4}{3}\left(\frac{1-\upsilon_1^2}{E_1} + \frac{1-\upsilon_2^2}{E_2} \right) \tag{6}$$

with ν_i and E_i (i=1,2) being Poisson's ratio and Young's modulus for the particle and surface, respectively.

As pointed out by Vainshtein (1997), the above equations describe particle resuspension from a smooth surface. However, most surfaces involved in resuspension are uneven or rough. This surface unevenness, or asperity, will act to reduce the particle adhesive force on that surface. To account for this effect in his model, Vainshtein adopts the quantity of surface asperity which is characterized by an asperity radius, r_a (m), which replaces the actual particle radius in Equation (5). Following Vainshtein, this asperity radius is normalized to the radius of the deposited particle:

$$r_a' = \frac{r_a}{R}. \tag{7}$$

The asperity radius, or normalized asperity radius, is assumed to have a surface distribution that follows a lognormal distribution, defined as

$$\varphi(r_a') = \frac{1}{(2\pi)^{1/2}} \frac{1}{r_a'} \frac{1}{\ln\sigma_a'} \exp\left(- \frac{\left(\ln r_a' - \ln \bar{r}_a'\right)^2}{2\left(\ln\sigma_a'\right)^2} \right) \tag{8}$$

where $\bar{r}_a'$ is the geometric mean of r_a', and is a measure of the reduction in adhesion due to surface asperity, and σ_a' is a measure of the spread in the surface adhesive force distribution. From Equations (6) through (8), it can be seen that the surface adhesive force will also have a lognormal distribution. Therefore if the surface adhesive force has a lognormal distribution, it would follow that the distribution of particles bound to this surface would also have the same distribution.

The mass fraction $F_R(t)$, defined as the mass, m (kg), on the surface at a given time divided by the initially deposited mass, m_o (kg), or m/m_o, of particles of radius R adhering to a given surface, can be found by integrating particle surface distribution (Equation (8)):

$$F_R(t) = \int_0^\infty \varphi\left(r_a', t\right) dr_a'. \tag{9}$$

Differentiating Equation (9) with respect to time gives the rate of change of the mass fraction of particles of radius R on the surface as

$$\frac{\partial F_R}{\partial t} = \int_0^\infty \frac{\partial \varphi\left(r_a', t\right)}{\partial t} dr_a'. \tag{10}$$

The deposition profile can change in time, $\frac{\partial \varphi(r_a', t)}{\partial t}$, as a result of particle resuspension. By substituting the asperity radius, r_a, in Equation (1) for particle radius, the resuspension rate constant, $p(r_a')$ (s^{-1}), of particles of radius R adhering to a given surface with a force that is proportional to the asperity radius, r_a, is obtained. This resuspension rate constant is related to the change in distribution profile by

$$\frac{\partial \varphi\left(r_a', t\right)}{\partial t} = - p(r_a') \varphi\left(r_a', t\right). \tag{11}$$

Upon substitution of Equation (11), Equation (10) now becomes

$$\frac{\partial F_R(t)}{\partial t} = - \int_0^\infty p\left(r_a'\right) \varphi\left(r_a', t\right) dr_a'. \tag{12}$$

The problem is now the integration of Equation (12) into a computer code like MELCOR to determine the desired mass resuspension rate of particles of radius R. First the integral of Equation (12) is approximated as the summation over discrete intervals in asperity radius, $\Delta r_a'$, which is the approach also adopted by Stempniewicz, Komen, and de With (2008). In equation form, this approximation can be written as

$$\frac{\partial F_R(t)}{\partial t} = -\int_0^\infty p\left(r_a'\right)\varphi\left(r_a', t\right)dr_a' \cong -\sum_{i=1}^{N} p\left(r_{a,i}'\right)\varphi\left(r_{a,i}', t\right)\Delta r_{a,i}' \tag{13}$$

where the subscript "*i*" represents quantities averaged over interval $\Delta r_{a,i}'$.

In selecting appropriate intervals, $\Delta r_{a,i}'$, that will give an accurate representation of the area under the lognormal distribution of Equation (8), we start by substituting

$$x = \frac{\ln r_a' - \ln \bar{r}_a'}{\ln \sigma_a'}, \tag{14}$$

which now gives

$$F_R = \frac{1}{(2\pi)^{1/2}} \int_{-\infty}^{\infty} \exp\left(-\frac{x^2}{2}\right) dx. \tag{15}$$

As can be seen, the result is the integral of a normal distribution which can be evaluated by use of the standard error function. Figure 1 shows a plot of the normal distribution divided into 41 equally-spaced intervals in *x*. It is clear from this figure that the intervals of integration should also be equally spaced in *x*, which in this case is proportional to $ln(r_a')$ (note Equation (14)). It can also be noted in Figure 1 that at *x* equals zero, or r_a' equals $\bar{r}_a'$, that the peak of the distribution occurs and that the interval -4 < x < 4 contains most of the area under this curve. Allowing for the approximation

$$F_R = \frac{1}{(2\pi)^{1/2}} \int_{-\infty}^{\infty} \exp\left(-\frac{x^2}{2}\right) dx \approx \frac{1}{(2\pi)^{1/2}} \sum_{i=1}^{N} \exp\left(-\frac{x_i^2}{2}\right)\Delta x_i = \sum_{i=1}^{N} \Delta F_{R\,i} \tag{16}$$

and noting that Equation (15) can be integrated accurately up to any value of *x*, by making use of

$$F_R(x) = \frac{1}{(2\pi)^{1/2}} \int_{-\infty}^{x} \exp\left(-\frac{t^2}{2}\right) dt = \frac{1}{2}\left(1 + sign(x) \times erf\left(\frac{|x|}{\sqrt{2}}\right)\right), \tag{17}$$

the fraction of particles, ΔF_{R_i} of Equation (16) that reside in interval Δx_i can be easily found from Equation (17) by evaluating $F_R(x)$ at $x_i+\Delta x_i$ and $x_i-\Delta x_i$, and subtracting the results.

Returning now to Equation (13), the rate of change of the mass fraction of particles of radius *R* can now be written as

$$\frac{\partial F_R(t)}{\partial t} = \sum_{i=1}^{N} \frac{\partial \Delta F_{Ri}(t)}{\partial t} = -\sum_{i=1}^{N} p(r_{a,i}')\Delta F_{R_i}(t). \tag{18}$$

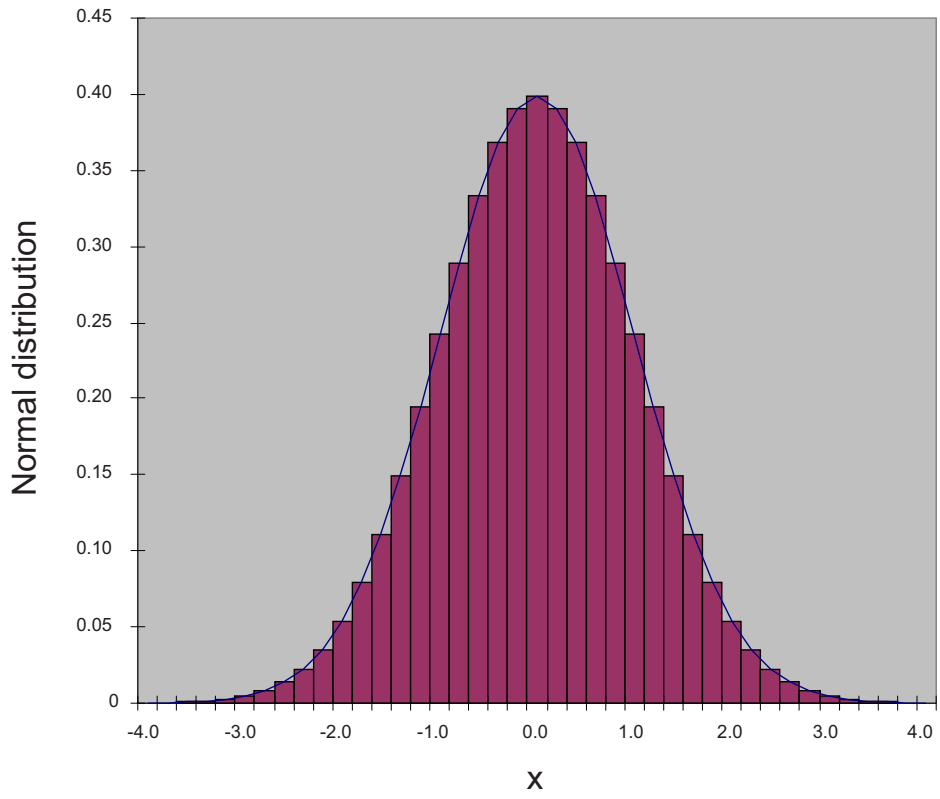

Figure 1. Plot of discretized normal distribution.

Individual terms of Equation (18) can be solved in finite difference form as

$$\frac{\Delta F_{R_i i}^{\,n+1} - \Delta F_{R_i i}^{\,n}}{\Delta t} = -p(r'_{a,i}) \times \left(\theta \times \Delta F_{R_i i}^{\,n+1} + (1-\theta) \times \Delta F_{R_i i}^{\,n}\right) \tag{19}$$

where Δt is the time-step size (s), θ is a numerical weighting parameter that sets the time advancement as anything from fully explicit (θ=0) to fully implicit (θ=1), and "n" represents the step interval. Once the particle masses, $\Delta F_{R_i}^{\,n+1}$, are update to the new time level, t^{n+1} (s), the fractions in all intervals can be summed to determine the total mass fraction remaining on the surface at the new time level, $F_R(t^{n+1})$.

What has been presented thus far gives the resuspension rate of a particle of a given radius. In reality, there will also be a distribution in particle size or radius. In codes such as MELCOR (Gauntt 2005), the particle size distribution is user-defined and can also be lognormal in nature. To account for this, intervals or bins by particle radius are defined to solve the integral-differential equations of particle mass transport and deposition. This bin structure must be defined for all structures upon which particle deposition can occur. Thus, to implement the above model, without some additional approximation, would require the definition of "n_R" particle radius intervals and "n_{ra}" asperity intervals, per each particle radius, for the number of surfaces, "n_s," in the problem, or $n_s \times n_R \times n_{ra}$ total intervals, which represents a sizeable computer memory requirement. To remedy this problem, the less tightly bound particles will be the first to undergo resuspension, which are the particles on the left in Figure 1. If the approximation is made that while mass resuspension is calculated in all intervals of Figure 1 that contain mass, but for tracking purposes the resuspended mass is leaving only a single "resuspension" interval from left to right in sequential order, then only a single parameter needs to be stored in memory, which is the time-dependent

mass fraction, F_R, calculated for each radius interval for a given surface. This changes the memory requirements from a total of $n_s \times n_R \times n_{ra}$ to $n_s \times 2n_R$. Advancing the mass fraction in time for a given particle radius on a given surface then requires only an initial interpolation of a standard asperity interval structure, which is common to all particle radii and surfaces, to determine the starting or resuspension interval at that point in time (that is, all intervals to the left of this starting interval will already be empty). The implication of this assumption is illustrated in graphical form in the next section.

3. VAINSHTEIN RESUSPENSION MODEL VALIDATION PROBLEM

3.1 Functional and Operational Objectives

Vainshtein et al. (1997) applied his resuspension model to flow conditions examined in Reeks (1988). These conditions are for the resuspension of spherical glass particles from a stainless steel substrate, exposed to fully-developed turbulent air flow in a channel. The relevant fluid and material properties for this application, as stated in Vainshtein et al. (1997), are listed in Table 1. For this test case, Vainshtein assumes that the mean asperity radius, $\bar{r}_a'$, is 0.1 and spread in adhesive force, σ_a', equals 4.

Table 1. Fluid and material properties used in Vainshtein test problem.

Particle density (kg/m^3)	ρ_p	2470
Fluid density (kg/m^3)	ρ_f	1.18
Substrate density (kg/m^3)	ρ_2	7800
Fluid viscosity (kg/m-s)	μ	1.82×10^{-5}
Surface energy (J/m^2)	$\Delta\gamma$	0.15
Particle Young's modulus (Pa)	E_1	8.01×10^{10}
Substrate Young's modulus (Pa)	E_2	2.15×10^{11}
Particle Poisson's ration	ν_1	0.27
Substrate Poisson's ratio	ν_2	0.28
Particle radius (μm)	R	20

Figure 2 shows the mass fraction distribution calculated from Equation (18) for this test problem after a 1-second exposure time to a flow with a frictional velocity of 1 m/s (note Figure 2a), compared to the distribution calculated from the approximation to Equation (18), which is tracking only $F_R(t)$ (note Figure 2b) where both solutions are using Vainshtein's resuspension rate constant. Ninety-nine mass fraction intervals were used for this problem. The effect of assuming that mass is mobilized from a single interval at a time is evident by comparing Figure 2a and 2b. This figure illustrates that more mass is being removed in the approximate approach from intervals to the left of the resuspension interval (at $x \cong -0.6$) in Figure 2b and less mass is being removed from bins to the right of this bin. In fact, in approximation 2b, mass is only being removed from one interval at a time, while the rate of resuspension from that interval equals the sum of the resuspension rates from all intervals to the right, including this resuspension interval in the approximate approach. While the approximation does miss the profile evolution in time, the end result of mass fraction remaining after a 1-second exposure time only differs by ~4% from the exact solution. For these conditions, the solution of Equation (18) gives a value of 0.69, while the approximation gives a value of 0.72.

Figure 3 presents a comparison of our Vainshtein resuspension model for MELCOR against the results obtained by Vainshtein et al. (1997) for this test problem. The points plotted representing Vainshtein's results were obtained by digitizing Figure 2 of Vainshtein et al. (1997), and not from any tabulation of results found in his paper. Based on the discussion in Vainshtein et al. (1997), the method Vainshtein used to solve Equation (19) of his paper and arrive at the results present in Figure 2 of this paper was not given. However, as can be seen, good agreement has been obtained for our approach against Vainshtein's results. It can also be seen that, for this problem, the approximate solution of Equation (18) using Vainshtein's resuspension rate constant is very close to the "exact" solution, and, given the uncertainty associated with the input parameters of this model, is an acceptable approximation.

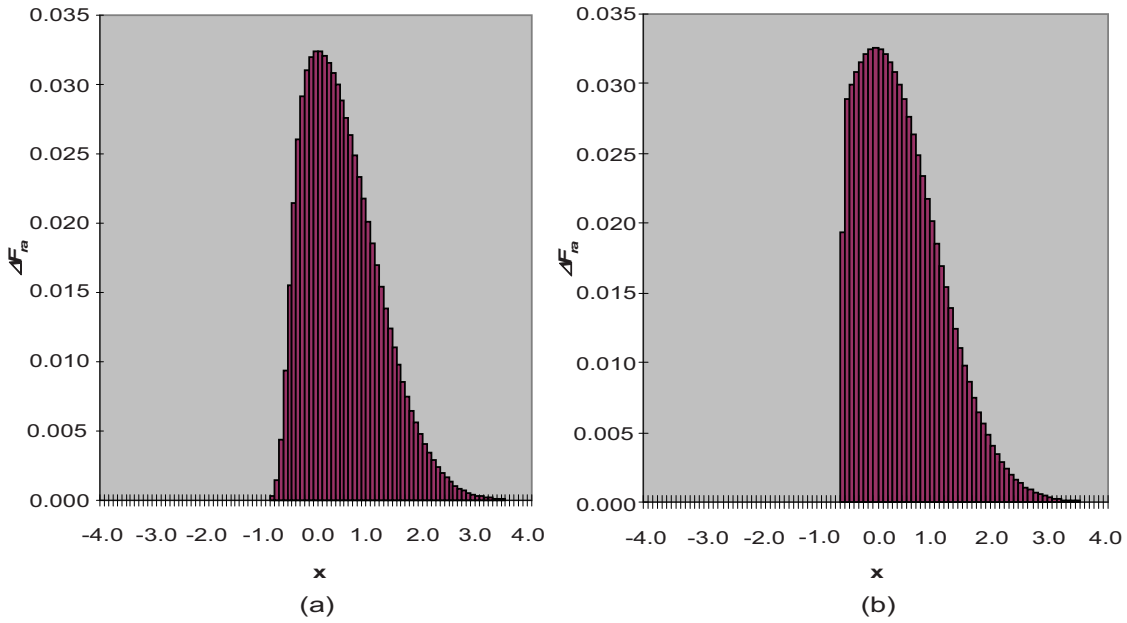

Figure 2. Particle mass fraction profile predicted after one second from Equation (18) and approximation of Equation (18).

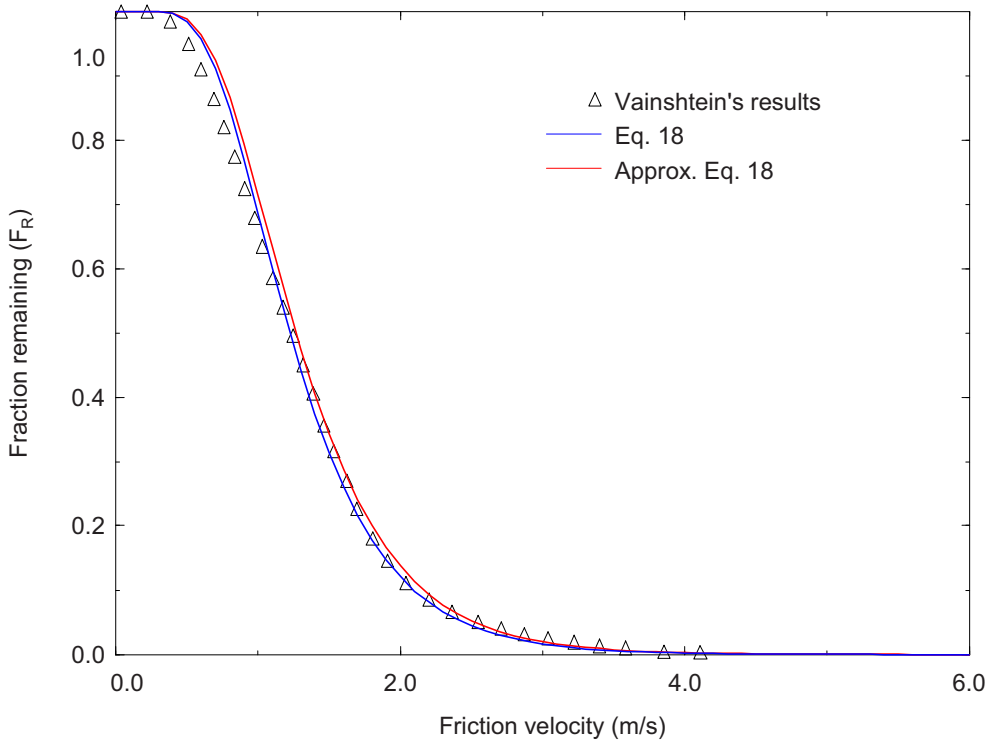

Figure 3. Comparison between results obtained by Vainshtein and solutions to Equation (18) with the Vainshtein resuspension rate constant.

4. ROCK 'N ROLL RESUSPENSION MODEL

The Rock 'n Roll resuspension model was developed by Reeks and Hall (2001). This model is a revision of a previous model developed by Reeks, Reed, and Hall (1988) known as the RRH model. The RRH model is based on a potential well model, as was the Vainshtein model presented in Section 1. In the RRH model, a particle energy balance is considered for which the kinetic energy of particle must exceed the potential energy well (surface adhesion) in which the particle resides before resuspension can occur. In this model, the center of the particle is assumed to oscillate vertically in the well until achieving the required kinetic energy to leave the well and become resuspended. In the Rock 'n Roll model, a particle is assumed to be in contact with the surface at two points of surface asperity. At the first point, the particle experiences the surface adhesive force. At the second point, called the pivot point and defined to be a distance 'a' from the adhesive point, the particle is restrained from lateral movement. In this model, the particle oscillates about the pivot point until it gains the kinetic energy required to break with the adhesive point. When this happens, it is assumed that the lift force on the particle is either sufficient to break contact with the pivot point, and the particle is resuspended, or it rolls along the surface until the adhesion force at a single-point of contact is sufficiently low to allow particle resuspension, thus the name the Rock 'n Roll model.

There are two Rock 'n Roll models presented in Reeks and Hall (2001), the dynamic and quasi-static resuspension models. The quasi-static model was adopted for MELCOR at this time because this model is a simplification of the dynamic model and is easier to implement. In the quasi-static model, the motion of the particles is driven by turbulent removal forces that are off-resonance with particle oscillation. Under this circumstance, the particle equation of motion can be approximated by a force balance between the aerodynamic removal forces and the surface adhesion forces. The particle resuspension rate constant, p (s^{-1}), derived by Reeks and Hall for these conditions is

$$p = n_\theta \exp\left(\frac{-\left(f_a - \langle F \rangle\right)^2}{2\langle f^2 \rangle} \right) / \frac{1}{2}\left\{ 1 + erf\left(\left(f_a - \langle F \rangle\right) / \sqrt{2\langle f^2 \rangle} \right) \right\} \tag{20}$$

where n_θ is the frequency of particle fluctuation (s^{-1}), defined as

$$n_\theta = 0.00658\left(\frac{u_\tau^2}{\nu_f} \right) \tag{21}$$

where ν_f is the fluid kinematic viscosity (m^2/s). The quantity f_a is the normalized surface adhesion force which is assumed, when normalized to the particle adhesive force for a smooth surface ($F_a = 3\pi \Delta\gamma R/2$), to have the lognormal surface distribution

$$\varphi(f_a') = \frac{1}{(2\pi)^{1/2}} \frac{1}{f_a'} \frac{1}{\ln\sigma_a'} \exp\left(-\frac{\left(\ln f_a' - \ln \bar{f}_a'\right)^2}{2\left(\ln\sigma_a'\right)^2} \right) \tag{22}$$

with the geometric mean, $\bar{f}_a'$, set to one. The quantity $<F>$ is the average aerodynamic force on a particle (N), and equals the time average of

$$F(t) = \frac{1}{2} F_L + \frac{R}{a} F_D \tag{23}$$

where F_L (N) and F_D (N) are the lift and drag force acting on the particle, respectively. The quantity $<f^2>$ (N^2) is the covariant of the fluctuating component of this aerodynamic force. Hall's (1998) measurements

show that the root-mean-square of a spherical particle's oscillation on a surface is proportional to the aerodynamic forces acting on that particle, as

$$\sqrt{\langle f^2 \rangle} = 0.2\langle F \rangle . \tag{24}$$

The average aerodynamic force, <F>, is obtained from Equation 23 by defining the average lift force as

$$\langle F_L \rangle = 20.9\rho_f \nu_f^2 \left(\frac{Ru_\tau}{\nu_f} \right)^{2.31} \tag{25}$$

demonstrated by Hall (1988), and the average drag force being 1.7 times the Stokes drag force (O'Neill 1968) on a spherical particle that is near or on the surface during laminar shear flow, which is appropriate for the laminar sublayer of turbulent flow. This force is defined as

$$\langle F_L \rangle = 32\rho_f \nu_f^2 \left(\frac{Ru_\tau}{\nu_f} \right)^2 . \tag{26}$$

Having defined the resuspension rate constant, Equation (18) can now be used to determine the particle mass fraction remaining on the surface as a function of time. This analysis is contained in the next section.

5. ROCK ‘N ROLL RESUSPENSION MODEL VALIDATION

Reeks and Hall (2001) compared the RRH and Rock ‘n Roll models to resuspension measurements for 10 and 20 μm alumina and graphite spherical particles. Figure 9 of this reference presents this comparison for 10 μm alumina spheres from three experimental test runs (Runs 9, 10, and 15). For this data comparison, the fitted adhesive values for these models are presented in Table 4 of this same reference. For the Rock ‘n Roll model, 10 μm alumina spheres have an interfacial surface energy of 0.56 J/m^2, an adhesive spread ($\sigma_a^{'}$) of 10.4, an adhesive reduction of 37, and a geometric factor (R/a) of 100. While it is not explicitly stated in Reeks and Hall (2001) it is assumed that results of Figure 9 are those obtained after an exposure time of 1 second. This exposure time was assumed because these same authors use this exposure time in discussing comparisons between the RRH and the two Rock ‘n Roll models in the text of their paper, plus in additional sensitivity calculations presented in their paper.

Figure 4 shows a comparison of data digitized from Figure 9 of Reeks and Hall (2001), compared to the results obtained from the approximate solution to Equation 18 using the quasi-static Rock ‘n Roll resuspension rate constant. For this comparison the exact and approximate solution to Equation (18) agree to within less than ~0.5%, so there is no need to present both solutions. As can be seen, very good agreement was obtained with our model.

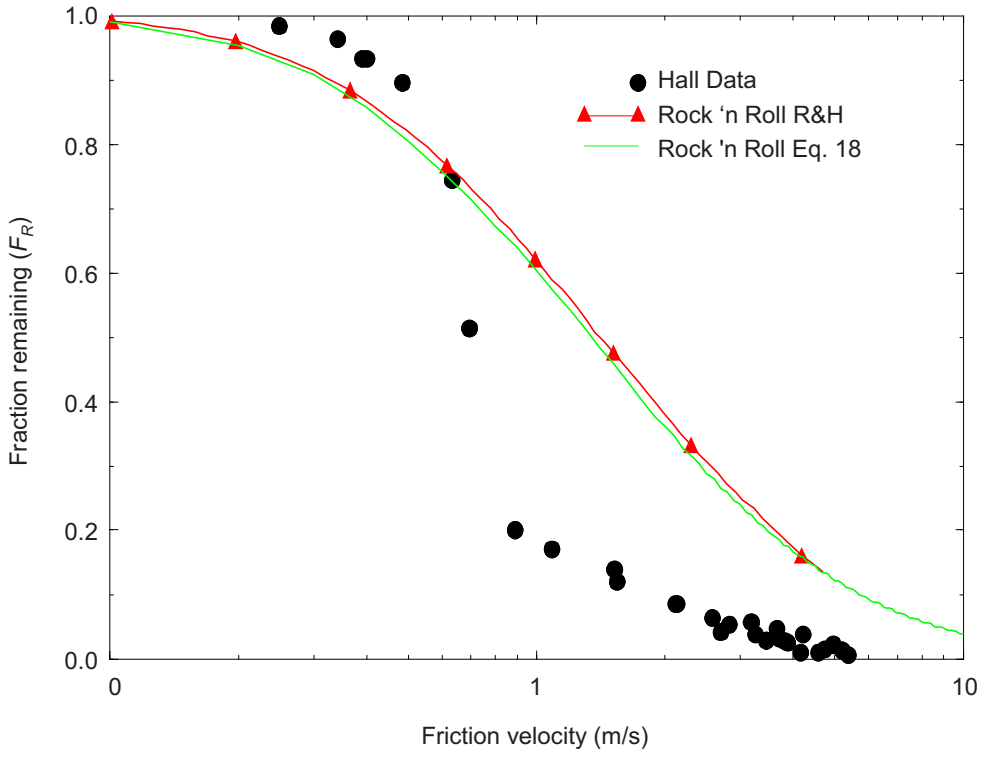

Figure 4. Comparison of results obtained by Reeks and Hall’s Rock n’ Roll model and a solution to Equation (18) with the Rock n’ Roll resuspension rate constant against data from Hall for 10 μm alumina spheres during Runs 9, 10, and 15.

6. FRICTION VELOCITY FORMULATION

Equation 3 relates the fluid tangential friction velocity to the fluid bulk velocity through the definition of the local friction factor or skin friction at the surface. The derivation of this equation starts from the definition of the friction velocity as

$$u_\tau \equiv \sqrt{\tau_o / \rho} \tag{27}$$

where τ_o is fluid shear stress at a wall surface (N), defined as

$$\tau_o = \mu \left. \frac{\partial V_f}{\partial y} \right|_{y=o} \tag{28}$$

and where y is the distance (m) into the laminar sublayer perpendicular to the surface. Given the definition of the coefficient of local skin friction as

$$C_f = \frac{\tau_o}{\rho V_f / 2}. \tag{29}$$

Equation 3 is obtained from Equation 27 by substitute for τ_o from the above definition of skin friction.

The implementation of our resuspension model in MELCOR requires the specification of the local skin friction for a given surface. This is done by taking advantage of the analogy between energy and momentum transfer at a surface, as discussed in Welty, Wicks, and Wilson (1969). The analogy adopted is the Colburn Analogy (1933), which relates surface local surface heat transfer coefficient, h (W/m^2-K), to the local skin friction as

$$C_f / 2 = St \, \mathrm{Pr}^{2/3} \tag{30}$$

where St and Pr are the fluid Stanton and Prandtl numbers, respectively, defined as

$$St \equiv \frac{h}{\rho V_f c_p} \tag{31}$$

and

$$\mathrm{Pr} \equiv \frac{\mu c_p}{k}. \tag{32}$$

The remaining parameters c_p and k are fluid heat capacity (J/kg-K) and thermal conductivity (W/m-K), respectively. With this analogy, the local skin friction coefficient can be directly determined for deposition surfaces in MELCOR from the code's heat transfer coefficient package predictions.

7. BIASI CORRELATION

Some material parameters in the Rock n' Roll model described above are difficult to measure in practice. Foremost among these are the mean $\bar{f}_a'$ and spread σ_a' of the normalized adhesive force distribution, which arise from the irregularity (at small scales) of the surfaces to which particles adhere. In order to rectify this difficulty, Biasi et al. (2001) proposed a method of estimating these parameters by correlating them with the particle size. He assembled the four published sets of experiment data, applied the Rock n' Roll model to each experiment, and adjusted $\bar{f}_a'$ and σ_a' so as to achieve the best match for each case. As the various experiments were carried out with particles of different composition and size, non-linear regression gave a correlation for both $\bar{f}_a'$ and σ_a' as a function of particle radius (in microns):

$$\bar{f}_a' = 0.016 - 0.0023 r^{0.545} \tag{33}$$

$$\sigma_a' = 1.8 + 0.136 r^{1.4}. \tag{34}$$

These correlations were then used in the Rock n' Roll model to model all of the experiments. Most of the experiment results for resuspension were within 20% of the model value, and all were within 30%, which is good agreement, considering the widely varying conditions of each experiment. Lacking any more direct measurement of these parameters, the Biasi correlation is recommended for use along with the Rock n' Roll model, and is applied in modeling the Simplified Test of Resuspension Mechanism (STORM) experiments discussed below.

8. DEPOSITED MASS PARTICLE SIZE DISTRIBUTION

Aerosol particles are not all one size, and in order to predict the total mass resuspended during an accident, resuspension rates for a range of particle sizes on a given surface must be considered. In equation form the total resuspension rate is written as

$$\frac{\partial F_T(t)}{\partial t} = \int_{R_p \min}^{R_p \max} P\left(R_p\right) \frac{\partial F_R(t)}{\partial t} dR_p \tag{35}$$

where, $R_{p,min}$ is the minimum particle radius (m) and $R_{p,min}$ is the maximum allowed particle radius (m). Often the particle size distribution, $P(R_p)$, can also be assumed to be a lognormal distribution.

MELCOR models aerosols in the atmosphere as having a size distribution (Gauntt 2005), and the transport of these particles occurs within user specified bins that vary in size between the minimum and maximum allowed particle radii. However, once these particles are deposited on a given surface their size distribution was no longer tracked and is lost. To remedy this problem, the same aerosol bin structure used by MELCOR to transport aerosol particles in the atmosphere was used to track the particle size distribution on deposition surfaces. This was done by modifying the MELCOR aerosol deposited mass arrays to reflect this bin structure. Now the rate of change with time of the total deposited mass of the 'k^{th}' MELCOR radionuclide material class on the 'j^{th}' MELCOR heat structure surface is obtained by summing (numerically integrating) the deposition rate minus the resuspension rate from each mass bin on that surface, which is given in equation form as

$$\frac{\partial M_{j,k}(t)}{\partial t} = \sum_{i=1}^{N} \{\Gamma_{i,k} - \frac{\partial F_{R,i}(t)}{\partial t} dM_{j,k}(R_i)\} \tag{36}$$

where $M_{j,k}(t)$ is the deposited mass (kg), N is the user specified number of aerosol bins, $\Gamma_{j,k}$ is the mass deposition rate (kg/s), and $dM_{j,k}(R_i)$ is the deposited mass (kg) of particles of radius R_i (m).

9. VERIFICATION OF RESUSPENSION MODEL IMPLEMENTATION IN MELCOR

9.1 Vainshtein Test Problem

The problem considered by Vainshtein, as described in Section 3 and illustrated in Figure 3, has been reproduced here along with a series of MELCOR runs using the Vainshtein model and parameters in Table 1. Figure 5 contains predictions from Vainshtein's article (Vainshtein et al. 1997) compared to those from the standalone and MELCOR codes: each point here indicates a separate MELCOR run at a different velocity (and corresponding friction velocity). The results labeled VZFG are digitized points from Figure 2 of Vainshtein et al. (1997). In figure 5, Vainshtein applied his resuspension model to flow conditions examined by Reeks (1988). These conditions are for the resuspension of spherical glass particles (R = 20 μm) from a stainless steel substrate, after being exposed for 1 second to fully-developed turbulent air flow with frictional velocities that vary from 0 to of 6 m/seconds. For this test case, Vainshtein assumes a mean asperity radius (r_a') of 0.1, an interfacial surface energy ($\Delta\gamma$) of 0.15 J/m^2, and a spread in adhesive force (σ_a') of 4. As can be seen, these results are in good agreement.

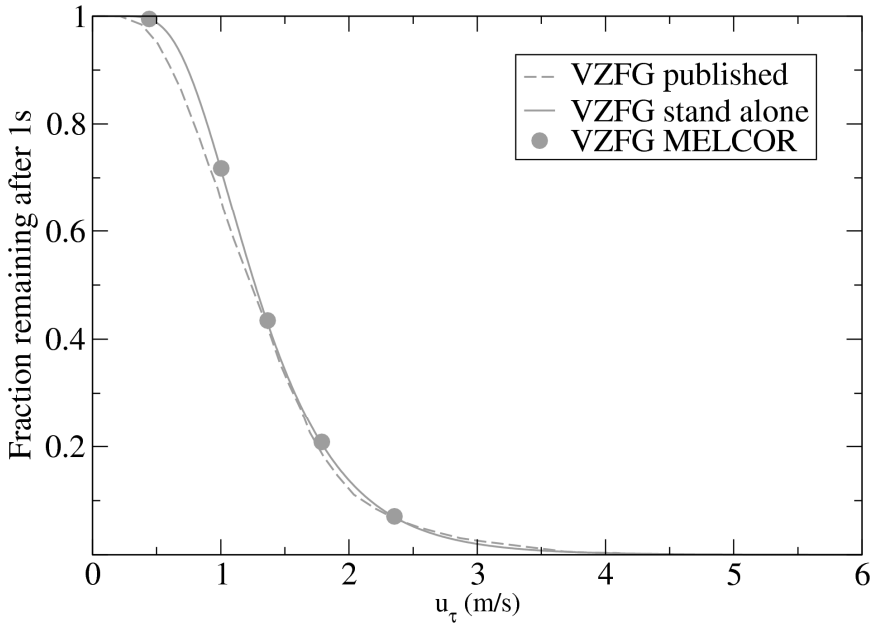

Figure 5. Comparison of results predicted from the VZFG model as obtained by the original author (Vainshtein et al. 1997), the stand alone code, and MELCOR.

9.2 Rock n' Roll test problems

Reeks and Hall (2001) compared their Rock 'n Roll models to resuspension measurements for 12.2 and 23 μm alumina and 13 μm graphite spherical particles from atop a stainless-steel surface. Figure 9 of Reeks and Hall (2001) presents a comparison for 12.2 μm alumina spheres from three experimental test runs (runs 9, 10, and 15). For this data comparison, the adopted parameters for their models is an interfacial surface energy of 0.56 J/m^2, an adhesive spread (σ_a') of 10.4, $\bar{f}_a'$ of 0.027, and a geometric factor (R/a) of 100. While it is not explicitly stated in Reeks and Hall (2001), it is assumed here that results of this figure are those obtained after an exposure time of 1 second, which was assumed because

these same authors use this exposure time in discussing comparisons between their resuspension models and additional sensitivity calculations presented in their paper.

Figure 6 contains the results of the comparison for 12.2 μm alumina particles. As was the case for Figure 5, the data presented and the original author's predictions have been digitized for Reeks and Hall (2001) and are reproduced in Figure 6. Also present are data from accompanying experiments performed by Reeks and Hall. As can be seen, the model's ability to reproduce the results found in Reeks and Hall (2001) is very good, giving confidence that the Rock 'n Roll resuspension model has been correctly replicated. This model agrees to within less than ~0.5% of digitized results. In addition, for completeness, the results predicted from the VZFG resuspension model is presented using the same material parameters as for the Rock 'n Roll model (Reeks and Hall 2001). At low frictional velocities, the VZFG under-predicts the resuspension rate. However, at higher frictional velocities the two models tend to reach better agreement.

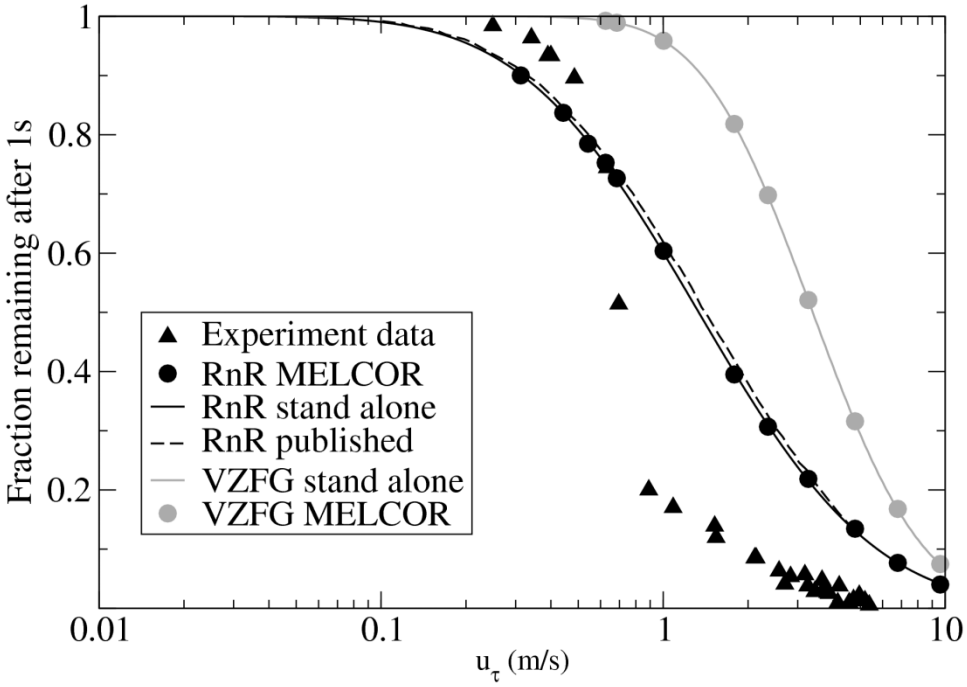

Figure 6. Comparison of experiment data (Reeks 2001) and predictions of the Rock 'n Roll model by the original author (Reeks 2001), the stand alone code, and MELCOR for 12.2 μm alumina particles. The VZFG model for the same material parameters is shown in gray.

A similar comparison for 23 μm alumina particles is shown in Figure 7. Since drag forces increase with the square of the particle radius, and adhesive forces only linearly, the larger alumina particles are more easily resuspended. Thus, the fraction remaining is smaller for the same value of u_τ in Figure 7. As before, the stand-alone and MELCOR implementations agree well with the published model.

The results for 13 μm graphite particles appear in Figure 8. Once again, the agreement with published results is excellent.

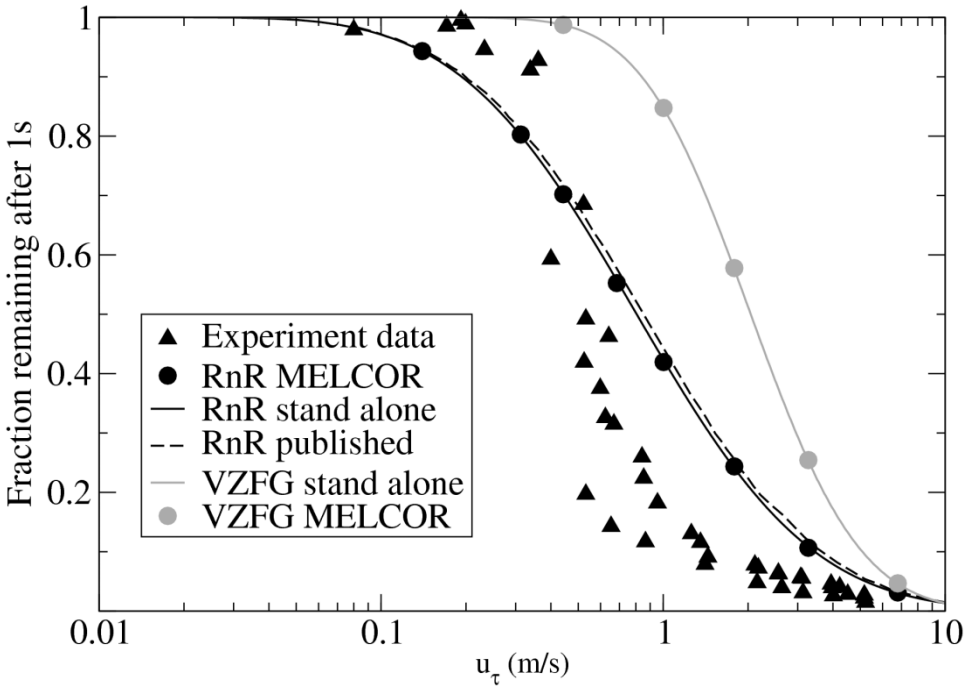

Figure 7. Comparison of experiment data (Reeks 2001) and predictions of the Rock 'n Roll model by the original author (Reeks 2001), the stand alone code, and MELCOR for 23 μm alumina particles. The VZFG model for the same material parameters is shown in gray.

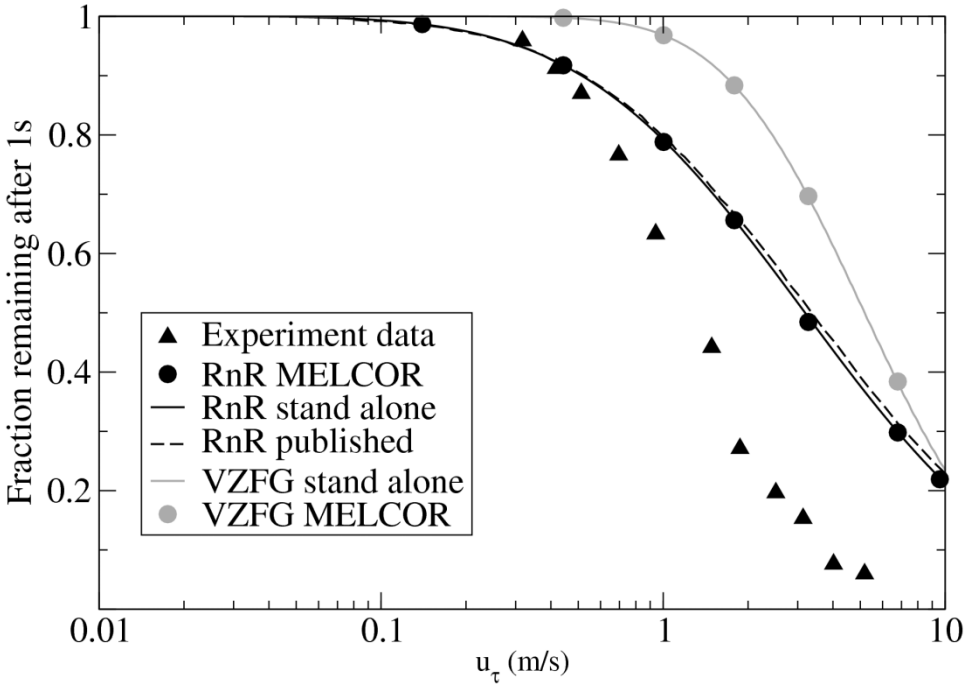

Figure 8. Comparison of experiment data (Reeks 2001) and predictions of the Rock 'n Roll model by the original author (Reeks 2001), the stand alone code, and MELCOR for 13 μm graphite particles. The VZFG model for the same material parameters is shown in gray.

9.3 Preliminary STORM Test Comparison

The STORM facility was operated by European Commission Joint Research Centre, Institute for Energy at Ispra, Varese, Italy. A schematic of this facility appears in Figure 9, as copied from Bujan (2010). The STORM test section was located downstream of a mixing vessel. The 63-mm inner diameter test section was 5 m long and was located within an oven to keep the test section wall temperature at the required levels during a test. For the resuspension tests in STORM, the tests proceeded in four phases: heat-up, temperature stabilization, aerosol deposition, and aerosol resuspension. During the aerosol deposition phase of a test, such as test SR11, the aerosol carrier gas flow velocity, typically <20 m/s, and temperature were maintained at levels that resulted in the primary mechanism for aerosol deposition being thermophoresis, with a smaller ~5% contribution by turbulent eddy impact deposition, and without any significant aerosol resuspension (Bujan 2010). During the resuspension phase, the temperature gradient between the carrier gas and the test section walls was reduced to as low as possible, and the carrier gas velocity was increased in steps according to the predetermined test plan (Castelo 1999). At the start of each velocity step increase, the filters that captured the resuspended aerosol mass were changed to allow the measurement of the mass resuspended during that particular velocity step. For STORM Test SR11, there were six velocity step increases as plotted in Figure 10.

A very simple MELCOR model of the STORM facility was developed for this comparison. This model contained only four control volumes that simulated the STORM mixing vessel, inlet pipe, test section, and outlet pipe. Heat structures were added to each of these volumes to allow for aerosol deposition in each volume. The model has four flow paths, two that connect the mixing vessel to the inlet pipe (flow during deposition phase of the test) and the test section (flow during the resuspension phase of a test). During the deposition phase of a test, an aerosol source is modeled in the inlet pipe, simulating the reported STORM aerosol mass injection rate during a given test. For test SR11, the aerosol injection rate was 3.83×10^{-4} kg/s of particles with a geometric mean diameter (GMD) of 0.43 μm.

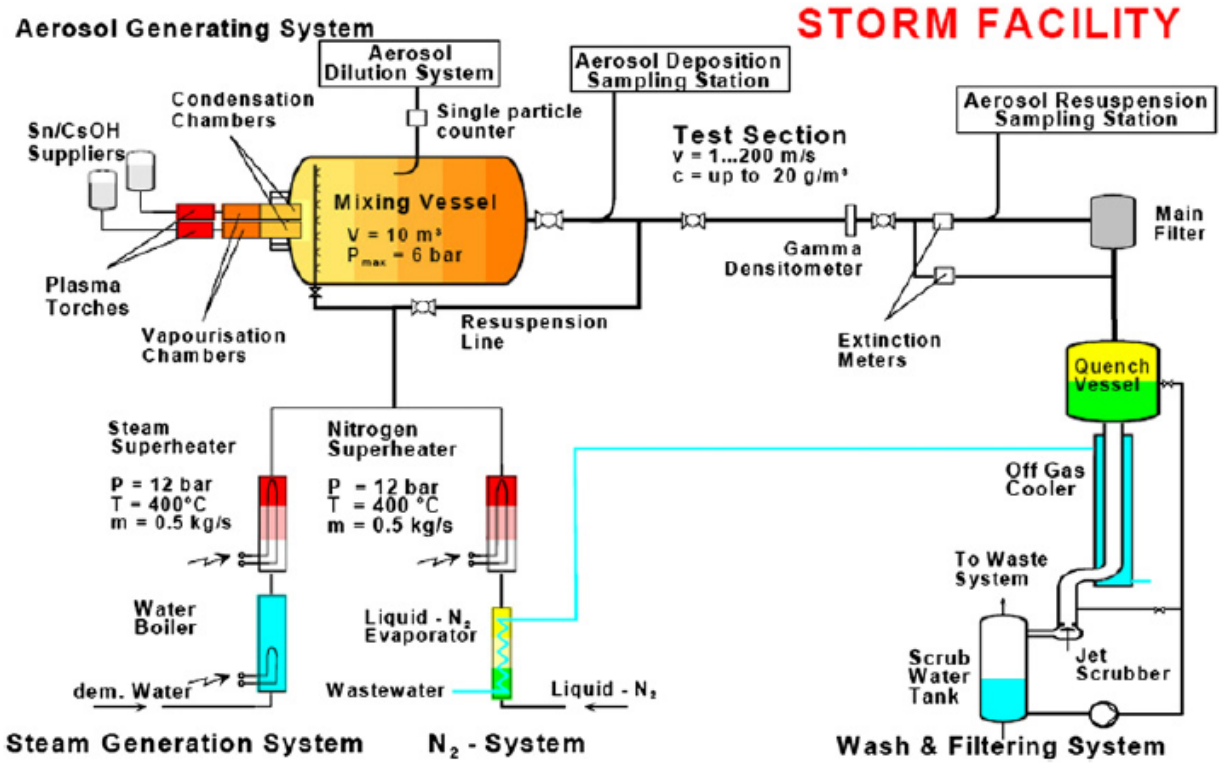

Figure 9. Schematic of STORM aerosol deposition and resuspension facility.

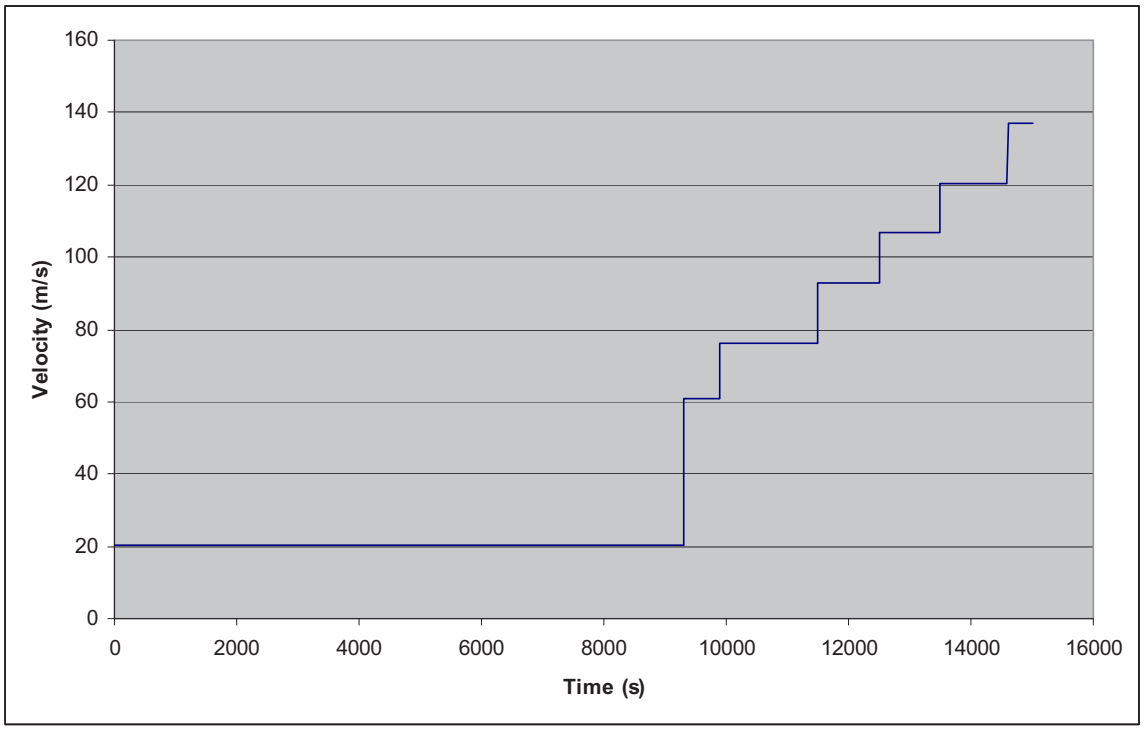

Figure 10. STORM aerosol deposition and resuspension test SR11 carrier gas velocity.

Figure 11 presents the MELCOR results for this test using the Rock n' Roll model with the Biasi correlation for particle adhesive parameters. Also presented in this figure are the measured results from STORM as contained in Castelo (1999). It is interesting to note that the reported aerosol mass deposited in the tests section was ~162 g, which is a small fraction of the more than 3 kg of aerosol mass that was transported through the test section during the deposition phase of this test. To allow MELCOR to arrive at approximately the same deposited mass through thermophoresis only, the particle dynamic shape factor was reduced from 1.0 to 0.8. This was required in part because MELCOR does not have a turbulent eddy impact deposition model. For this test, the MELCOR resuspension model predicted the overall mass resuspension fraction with good accuracy. The test measurements indicated that 71% of the deposited mass would be resuspended, while this MELCOR resuspension model predicted that 78% would be resuspended. When comparing the transient resuspension, the test data indicates a slower resuspension rate during the initial velocity steps and a more rapid resuspension rate during the latter velocity steps. This remains somewhat of a mystery at this time. The resuspension behavior predicted by MELCOR conforms to theory as specified in previous sections, that is at low velocities the less tightly bound particles will be readily resuspended, and as the velocity steps increase, the resuspension rate should be commensurately less per velocity step because the particles that remain are more tightly bound to the surface. The data seems to almost suggest the opposite trend. There could be some hint in the reported data of GMD for the resuspended particle. Not only were the resuspended particles larger than the original deposited particles (0.43 μm), but the size distribution was bimodal with GMD peaks at ~4 and ~1 μm, respectively. This result will be investigated further in future work.

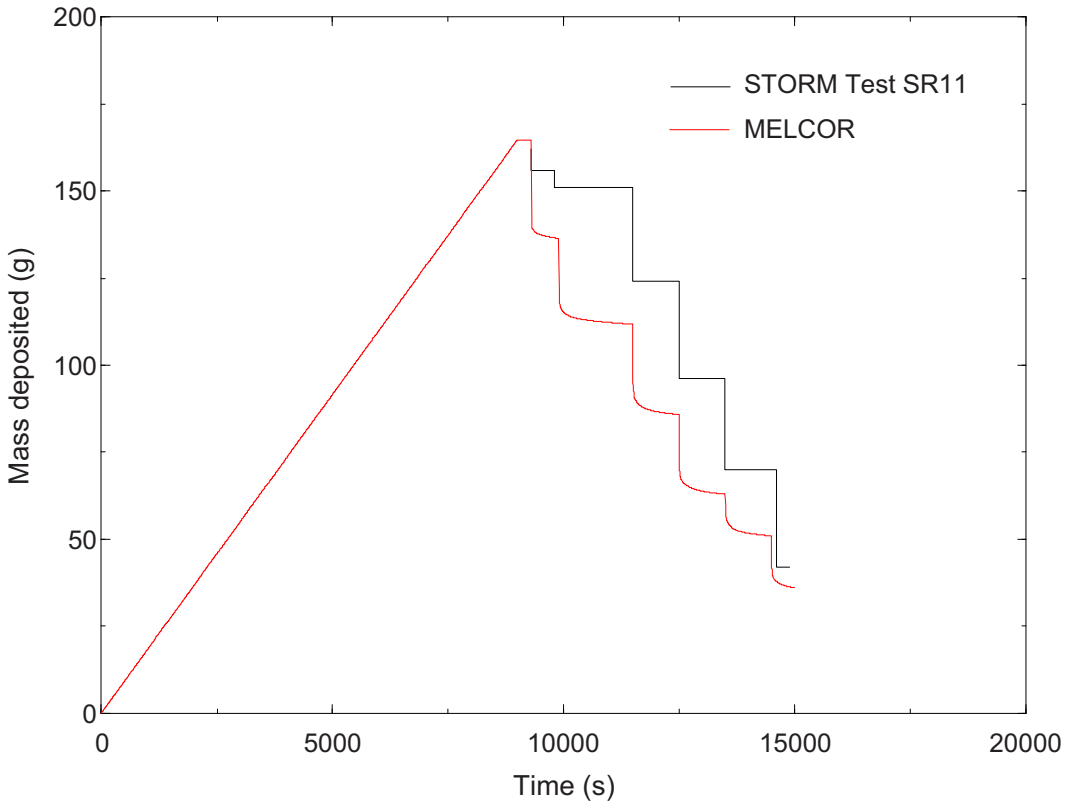

Figure 11. Comparison of MELCOR Rock n' Roll resuspension model with STORM Test SR11 resuspension data.

Bujan (2010) reports data from other STORM resuspension tests that make sense: SR12 and SR13. Bujan (2010) also presents data from Tests SR09 and SR10. However, Test SR09 reportedly had approximately the same mass deposited on the test section surface as did Tests SR11, SR12, and SR13, with a reported temperature gradient (gas-to-wall) for Test SR09 that was 40% less than those of Tests SR11 through SR13. Because thermophoresis is thought to be the dominant deposition mechanism, and this mechanism is linearly proportional to temperature gradient, the result from SR09 seems suspect. Regarding Test SR10, the reported resuspension fraction is 70% and a velocity increase that was only 65% of the overall velocity increase experienced in Test SR11, which only achieved a mass resuspension fraction of 74%. Because resuspension should increase dramatically with increasing velocity, the result for Test SR10 also seems suspect. However, for Test SR12, the reported resuspension fraction was ~51%, which compares to MELCOR resuspension model prediction of 61%. For SR13, the reported resuspension fraction was 8.5%, while for MELCOR the fraction was 16%. Therefore the results for Tests SR12 and SR13 also appear to be in agreement with our MELCOR resuspension model.

10. CONCLUSIONS

The kinetic particle resuspension models of Vainshtein et al. (1997) and Reeks and Hall (2001) have been implemented as a stand-alone code and as a subroutine in MELCOR. A MELCOR model of the experiment of Reeks and Hall (2001) was developed, and the results of the model agree well with the published model data of Vainshtein (1997) and Reeks (2001).

Biasi et al. (2001) has provided correlations for the adhesive force distribution parameters $\bar{f}_a'$ and σ_a' as a function of particle radius. These parameters influence the resuspension model significantly, but are difficult to determine in practice. This correlation has been implemented as an option for the Rock n' Roll resuspension model, and was applied in a MELCOR model of the STORM experiments (Castelo 1999). The MELCOR results are in good agreement with STORM Tests SR11 through SR13. Given some unphysical results of the other STORM tests, and the dearth of resuspension data in general, new experiment data would be of considerable value for further model validation.

11. REFERENCES

Biasi, L., A. de los Reyes, M. W. Reeks, and G. F. de Santi, 2001, "Use of a simple model for the interpretation of experimental data on particle resuspension in turbulent flows," *Aerosol Science*, Vol. 32, pp. 1175–1200.

Bujan A., L. Ammirabile, A. Bieliauskas, and B. Toth, 2010, "ASTEC V1.3 code SOPHAEROS module validation using the STORM experiments," *Progress in Nuclear Energy*, Vol. 52, pp. 777–788.

Castelo, A., F. A. Capitao, G. Santi, 1999, International Standard Problem 40 Aerosol Deposition and Resuspension Final Comparison Report, *European Commission Joint Research Centre Report*, *EUR 18708 EN*.

Colburn, A. P., 1933, "A method of correlating forced convection heat transfer data and a comparison with fluid friction," *Transaction of American Institute of Chemical Engineering*, Vol. 29.

Hall, D., 1988, "Measurements of the mean lift force on a particle near a boundary layer in turbulent flow," *Fluid Mechanics*, Vol. 187, p. 451.

Hall, D., 1998, "Measurements of the fluctuating lift force on a particle at a boundary in turbulent flow," *Journal of Experimental Fluids*, submitted.

Gauntt, R. O., et al.. 2005, "MELCOR Computer Code Manuals Vol. 1: Primer and Users' Guide Version 1.8.6," NUREG/CR-6119, Vol. 1, Rev.3, Sandia National Laboratory.

Merrill, B. J., 2008, Applicability of MELCOR for Use in Analyzing Air Ingress Accidents in a South African Pebble Bed Modular Reactor (PBMR)," INL/EXT-10-17658, INL.

Merrill, B. J., P. W. Humrickhouse, R. L. Moore, 2009, *A Comparison of Modifications to MELCOR Versions 1.8.2 and 1.8.6 for ITER Safety Analysis*, INL/EXT-09-16715, INL.

O'Neill, M. E., 1968, "A sphere in contact with a plane wall in a slow linear shear flow," *Chemical Engineering Science*, Vol. 23, pp. 1293–1298.

Reeks, M. W., J. R. Reed, and D. Hall, 1988, "The resuspension of small particles by turbulent flow," *Journal of Physics D*, Vol. 21, pp. 574–589.

Reeks, M. W., and D. Hall, 2001, "Kinetics models for particle resuspension in turbulent flows: theory and measurement," *Aerosol Science*, Vol. 32, pp. 1–31.

Stempniewicz, M. M., E. M. J. Komen, A. de With, 2008 "Model of particle resuspension in turbulent flows," *Nuclear Engineering and Design*, Vol. 238, pp. 2943–2959.

Vainshtein, P., B. Ziskind, M. Fichman, and C. Gutfinger, 1997, "Kinetic model of particle resuspension by a drag force," *Physical Review Letters*, Vol. 78, Issue 3, pp. 551–554.

Welty, J. R, C. E. Wicks, and R. E. Wilson, 1969, *Fundamentals of Momentum, Heat and Mass Transfer*, John Wiley & Sons, New York, New York , pp. 320–329.

Appendix A

MELCOR Resuspension Model Use

Appendix A
MELCOR Resuspension Model Use

A-1. Syntax

The standalone models for the Vainshtein and Rock n' Roll models described above (using the approximation discussed in Section 3) have been implemented as subroutines in MELCOR. The subroutines are invoked by including the RNARXXX records in the MELCOR input. For example:

```
rnar000 6
rnar001 0.027 10.4
```

The first line specifies the resuspension model to be used. Option 5 selects the Vainshtein model, Option 6 selects the Rock n' Roll model, and Option 7 selects the Rock n' Roll model with Biasi correlation. The second line provides the parameters of the adhesive force distribution. The first parameter on this line is the geometric mean of the nondimensional adhesive force distribution. Entering a positive value for this parameter selects alumina particles, while a negative value selects graphite particles. These are the only materials presently available. The second parameter on this line is the spread in the lognormal force distribution. If the Biasi correlation has been selected, these parameters are calculated from it, and input on the second line is ignored. Other parameters, such as the elastic properties of the particles and substrate, are presently hard-coded, as the RNARXXX record only accepts two parameters. Expanding this would require more extensive modification, which will be investigated for subsequent versions of MELCOR.

A-2. Notes on Friction Velocity

Above we have presented MELCOR results for the remaining particle fraction as a function of friction velocity, as is customary in the literature on this topic. Though determination of the friction velocity is not discussed by Vainshtein (1997) or Reeks and Hall (2001), the results of the Colburn analogy (1933) used in MELCOR are considered here. Heat structures in MELCOR are specified as either internal or external for the purposes of heat transfer calculations, and each can have either a rectangular or cylindrical geometry. The combination of these options determines the heat transfer correlation used. The experiments of Reeks and Hall (2001) were carried out in a rectangular duct, so an internal, rectangular heat structure best describes the geometry of these experiments. However, a plot of u_τ versus velocity, shown in Figure A.1 for this configuration, reveals an unexpected change in slope and poor agreement with the relationship obtained from the Fanning friction factor, which does not occur for a cylindrical heat structure of the same hydraulic diameter. The reason for this is, while the specification of a rectangular structure selects a correlation appropriate for internal flow, the turbulence transition point is taken for an *external* (flat plate) flow. This issue may be addressed in a future version of MELCOR, but present users need to be aware of the discrepancy.

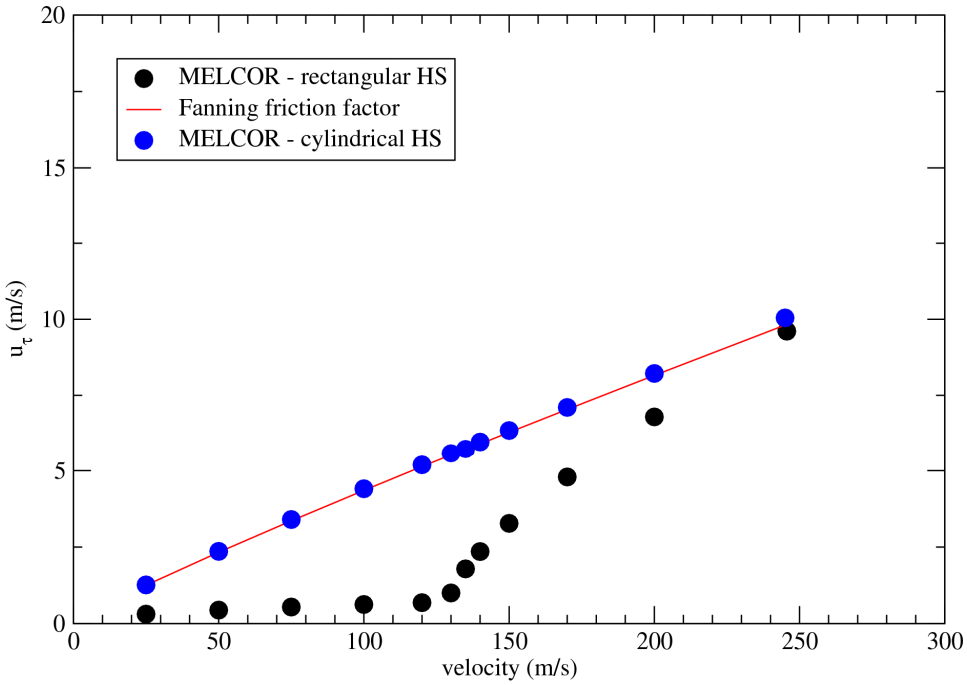

Figure A.1. Friction velocity calculated using the Colburn analogy (1933) in the heat transfer package of MELCOR, for cylindrical and rectangular heat structures (internal flow), compared with the Fanning friction factor.